Journal of Molecular Graphics and Modelling 66 (2016) 20–25

Contents lists available at ScienceDirect

Journal of Molecular Graphics and Modelling

journal homepage: www.elsevier.com/locate/JMGM

Charge-tunable insertion process of carbon nanotubes into DNA nanotubes

Lijun Liang[a,b], Zhisen Zhang[c], Zhe Kong[d], Yong Liu[e], Jia-Wei Shen[e,*], Debing Li[a], Qi Wang[b,*]

[a] College of Life Information Science and Instrument Engineering, Hangzhou Dianzi University, Hangzhou, People's Republic of China
[b] Department of Chemistry, Zhejiang University, Hangzhou 310027, People's Republic of China
[c] Research Institute for Soft Matter and Biomimetics, Department of Physics, Xiamen University, Xiamen 361005, People's Republic of China
[d] College of Materials and Environmental Engineering, Hangzhou Dianzi University, Hangzhou 310018, People's Republic of China
[e] School of Medicine, Hangzhou Normal University, Hangzhou 310016, People's Republic of China

ARTICLE INFO

Article history:
Received 3 February 2016
Received in revised form 20 March 2016
Accepted 22 March 2016
Available online 23 March 2016

Keywords:
Carbon nanotube
DNA nanotube
Self-assembly
Hybrid inorganic–organic nanomaterials

ABSTRACT

Control over interactions with biomolecules holds the key of the applications of carbon nanotubes (CNTs) in biotechnology. Here we report a molecule dynamics study on the encapsulation process of different charged CNTs into DNA nanotubes. Our results demonstrated that insertion process of CNTs into DNA nanotubes are charge-tunable. The positive charged CNTs could spontaneously encapsulate and confined in the hollow of DNA nanotubes under the combination of electrostatic and vdW interaction in our *ns* scale simulation. The conformation of DNA nanotubes is very stable even after the insertion of CNTs. For pristine CNTs, it could not entirely encapsulated by DNA nanotubes in simulation scale in this study. The encapsulation time of pristine CNTs into DNA nanotubes was estimated about 21.9 s based on the potential of mean force along the reaction coordination of encapsulation process of CNTs into DNA nanotubes. In addition, the encapsulation process was also affected by the diameter of CNTs. These findings highlight the charge-tunable self-assembly process of nanomaterials and biomolecules. Our study suggests that the encapsulated CNTs-DNA nanotubes could be used as building blocks for constructing organic–inorganic hybrid materials and has the potential applications in the field of biosensor, drug delivery system and biomaterials etc.

1. Introduction

Organic–inorganic hybrid materials do not represent only a creative alternative to design new materials and compounds for academic research, but their unusual features also promote the development of innovative industrial applications [1–3]. Recently, DNA nanotechnology has aroused much attention since its inception work by Seeman in 1982 [4]. Self-assembly nanotubes made from carbon [5–8], peptide [9–11] and DNA [12–15] has been thought as the potential building blocks for constructing the larger hierarchical structure. With the development of the self-assembly technology, the DNA nanotubes structure with particularly precise control have been fabricated [16–19]. It provides a new era to construct active materials with controlled nanoscale motion, dynamics and reconfiguration [20]. Especially, the functionalization of DNA nanotubes has been developed to serve as the templates for the assembly of the other materials [21,22]. However, the enhancement of mechanical property of DNA nanostructure is necessary to expand the scope of its potential applications [20,23–25]. For example, the improved resolution in force spectroscopy to detect DNA-protein interaction could be obtained with the improvement of the mechanical property of DNA nanostructure [26]. One way to enhance the mechanical property of DNA nanotubes is to make them composite material, and it could be achieved if DNA nanotubes hybrid with inorganic material.

Carbon nanotubes (CNTs) has attracted considerable attention due to its unique electric and mechanical properties from its first discovery in 1991 [27]. Extension research on application of CNT-based materials including nano-electronics, energy-storages, biotechnology and medicinal chemical has shown tremendous promises that CNTs could serve as an excellent building block [28–31]. Especially, CNTs have been used as building blocks to fabricate room temperature field-effect transistors [32], diode [33] etc.

* Corresponding authors.
E-mail addresses: shen.jiawei@hotmail.com (J.-W. Shen), qiwang@zju.edu.cn (Q. Wang).

http://dx.doi.org/10.1016/j.jmgm.2016.03.006
1093-3263/

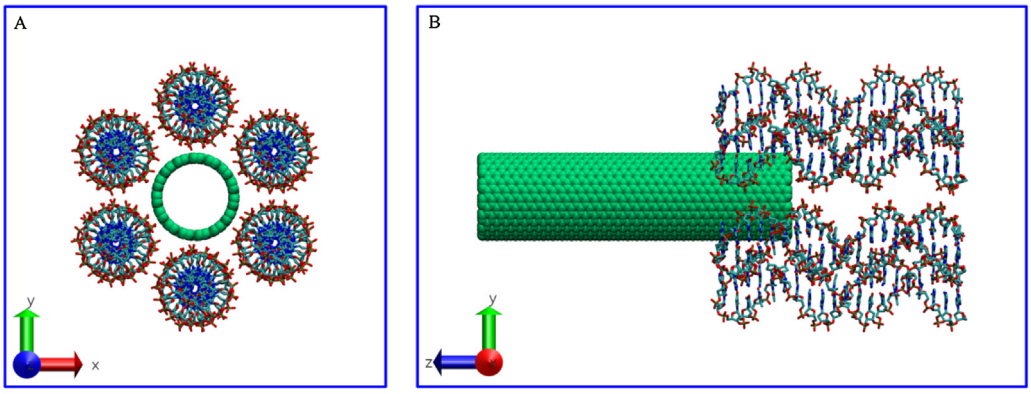

Fig. 1. Initial structure for CNTs (15, 15) in the DNA nanotubes. (A) the top view; (B) the side view. The DNA molecules are shown by CPK and ribbon model, and CNT are show in vdW model with green color. The water molecules and ions are not shown for clarity. (For interpretation of the references to color in this figure legend, the reader is referred to the web version of this article.)

Many studies both from experimental [34,35] and theoretical works [36,37] have been explored on the interaction of CNT and DNA. These works greatly enhance our understanding of the properties of CNT in the interaction between CNT and DNA. In addition, both of CNT and DNA nanotubes have been investigated as drug delivery in recent years [38,39]. However, as two important building blocks for novel organic–inorganic hybrid materials, the interaction between CNT and DNA nanotubes at the molecular level are still obscure. Especially, the dynamics of self-assembly process of DNA nanotubes and CNTs need to be better understood, which is very crucial for hybrid CNT-DNA nanotubes materials as a building block for novel organic–inorganic materials. Herein, we report a molecular dynamics simulation study on the dynamics of encapsulation process of CNTs into the hollow of DNA nanotubes in a water soluble environment. Our results demonstrated that insertion process of CNTs into DNA nanotubes are charge-tunable. The positive charged CNTs could spontaneously encapsulate and confined in the hollow of DNA nanotubes under the combination of electrostatic and vdW interaction but not neutral CNTs in our ns scale simulation. The time scale of insertion process of neutral CNTs into DNA nanotubes is estimated based on the potential of mean force (PMF). In addition, the structure of DNA nanotubes is very stable even after the encapsulation of CNTs into its hollow.

2. Methods

2.1. System setup

The armchair (6, 6) and (15, 15) CNTs were constructed by visual molecular dynamics (VMD) tool [40]. The diameters of two CNTs are 0.81 nm and 2.03 nm with the length of 8.00 nm, respectively. The vertical axis of two CNTs is along z direction. The surface charge densities considered in this work are rather realistic; for example, depending on the fabrication procedures [41], the charge density of a silica surface can vary between 0 and -5 e/nm^2. The charge density modified carbon-based materials had also been used in other theoretical works [42,43]. Both two types of CNTs were modified with different charge density (σ) varied from $\sigma = -0.5$ e/nm^2 for negative CNTs to $+0.5$ e/nm^2 for positive CNTs. Here, e denotes the charge of a proton. The charge density $\sigma = q/A$, where q is the total charge in the modified CNTs, and A represents the surface area of modified CNTs. With different size of CNTs diameter, the surface area in CNT (6, 6) and CNT (15, 15) is different. The total charges were $-13e$, $0e$ and $13e$ in the systems with negative, pristine and positive CNT (6, 6) before adding water and counterions. The charges were $-45e$, $0e$ and $45e$ in the systems with negative, pristine and positive CNT (15, 15) before adding water and counterions.

Double strands DNA (dsDNA) molecule with the sequence of poly(AT)$_{20}$ was constructed by Hyperchem (Version 7.0, Hypercube, Inc), and it was equilibrated for 1 ns in vacuum. The hexamer DNA nanotubes are designed based on DNA origami object, as shown in reference [44]. The center-of-mass (COM) of all six DNA molecules were placed in one regular hexagon in x-y plane, and the side length of regular hexagon is 2.31 nm. Na^+ ions or Cl^- ions was added into the water box to neutralize the system. Then 100 ns NVT ensemble simulation were performed to equilibrate the system. The structure of hexamer DNA nanotubes at the final state of the equilibration was exacted as the initial structure for investigating the encapsulation process of CNTs into DNA nanotubes. Position restrains of DNA nanotubes in x, y and z dimensions were used, and the force constant is 50 kJ mol^{-1} nm^{-2}. To investigate the effect of restrains of DNA nanotubes in the simulation, the simulaiton including DNA nanotubes without the restrains was also performed. The vertical axis of DNA nanotubes coincides with the vertical axis of CNTs, which is z axis. To accelerate the insertion process, 1.0 nm length of CNTs was inserted into the DNA nanotubes at the beginning of the equilibration, as shown in Fig. 1B. In most cases, the water box is $10.00 \times 10.00 \times 21.00$ nm^3 in the x, y and z directions, and 49566 TIP3 P water molecules were added into the box with system density of 1.001 g/cm^3. The buffer lenghs is 4 nm in z directon, and it is long enough to avoid the interaction with its periodic image. At last, Na^+ or Cl^- ions were added into the solution to neutralize the system, and the total atoms are around 157,000.

2.2. System simulation

The DNA molecules, Na^+ and Cl^- ions were modeled by the Charmm27 force field. The force field parameters of carbon atoms in CNTs were $\sigma_{CC} = 0.385$ nm and $\varepsilon_{CC} = 0.439$ kJ mol^{-1}, as used in previous works [45–48]. All atoms including hydrogen atoms were represented explicitly, and the bonds with hydrogen atom were constrained by LINCS algorithm. The cutoff for the non-bonded van der Waals interaction was set by a switching function starting at 1.0 nm and reaching zero at 1.2 nm. The Particle mesh Ewald (PME) summation [49] was used to calculate the long-ranged electrostatic interactions, with a cutoff distance of 1.2 nm for the separation of the direct and reciprocal space. All simulations were performed by Gromacs-5.0.4 program with the time step of 2 fs. Periodic boundary conditions (PBC) were applied in all MD simulations. After 10 ns equilibration, all MD simulations were carried out in NPT ensemble, and the Langevin method was employed to keep the temperature at 298 K and the pressure at 101.3 kPa, respectively.

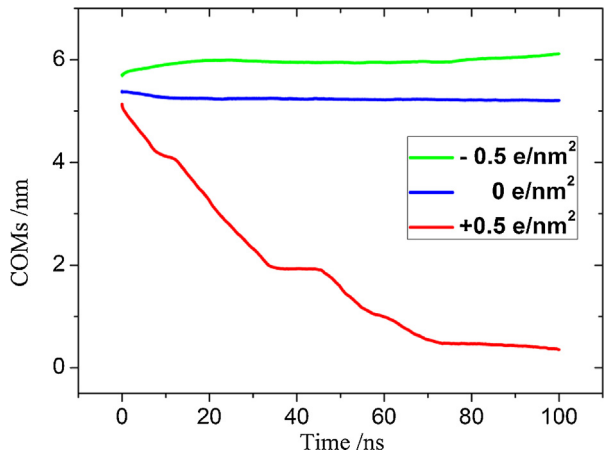

Fig. 2. Evolution of the COM distance between CNT (15, 15) with different charge density and DNA nanotubes: negative charged CNT, pristine CNT, and positive charged CNT. (For interpretation of the references to color in the text, the reader is referred to the web version of this article.)

3. Results and discussion

Fig. 2 shows the evolution of the COM distance between CNT (15, 15) with different charge density and DNA nanotubes. After 10 ns equilibration, the initial structures of all systems in MD were slightly different. The COM distance between pristine CNT and DNA nanotubes (blue line) has been slightly decreased. It decreased from 5.57 nm to 5.23 nm after 20 ns simulation. It indicates that a small part of the pristine CNT could enter into the DNA nanotubes. However, after that, the COM distance only decreased a little until the end of the simulation. It shows that pristine CNT is trapped in this region and it could not completely enter into the DNA nanotubes during the simulation time in this study. These founding imply that the self-assembly of the pristine CNT into DNA nanotubes is a relatively long process. In the system contain negative charged CNT and DNA nanotubes, the COM distance between negative charged CNTs and DNA nanotubes is 5.50 nm in the initial of the simulation, and it increases to 6.02 nm after 40 ns simulation, as seen in Fig. 2 (green line). It implied that the negatively charged CNTs had been repelled by DNA nanotubes. The negative CNTs could not enter into the DNA nanotubes because the DNA is natural negative charge. The distance between CNT with positive charge and DNA nanotubes decreased greatly until the CNTs completely encapsulated into the DNA nanotubes. As displayed in Fig. 2 (red line), during first 30 ns, the velocity of positive charged CNTs inserting into DNA nanotubes is almost constant, which is around 0.11 nm/ns. After half of positive charged CNTs entered into the DNA nanotubes, the CNT stay in that region for about 15 ns. Then, the positive charged CNTs enters into DNA nanotubes with a velocity around 0.06 nm/ns until the CNTs are encapsulated by DNA nanotubes completely. These results clearly show that the positive charged CNTs could spontaneously encapsulate into the DNA nanotubes but not for negative charged CNTs.

To enhance the understanding of the insertion process, the evolution of interaction energy (ΔE) between DNA and different charged CNTs were calculated in the simulation. As seen in Fig. S1 (in the supporting information), the interaction energy between DNA nanotubes and negative, neutral and positive CNTs decreases much in the simulation. It implicated that the insertion process of positive CNT into DNA nanotubes is electrostatic interaction driven. In addition, as seen in Fig. 3A, the average interaction energy between DNA nanotubes and negative, neutral and positive CNTs is −72.1, −356.2 and −2382.4 kJ mol^{-1} during last 10.0 ns simulation. It shows us the positive charged CNTs is very stable in the interior of DNA nanotubes.

After the insertion process of different charged CNT into DNA nanotubes, the structure of DNA nanotubes were investigated. As seen in Fig. 3B, the diameters of DNA nanotubes changed little in all systems (see Supporting Information Section I). The diameter of DNA nanotubes is about 4.95 nm, 4.83 nm and 4.72 nm in the systems with negative charged CNTs, neutral CNTs and positive charged CNTs, respectively. In the systems with neutral CNTs and positive charged CNTs, the diameter of DNA nanotubes decrease a little. The diameter of DNA nanotubes only decrease to 4.72 nm even after the whole positive charged CNT encapsulated into the DNA nanotubes. It indicates that the DNA nanotubes could adsorb with the neutral and positive charged CNTs. It could also be confirmed from the interaction energy between DNA nanotubes and CNTs. The interaction energy has increased much with the change of charge density on CNTs from negative to positive. However, the RMSDs of DNA nanotubes in three different systems are almost the same (data is not shown), and all of them are less than 0.05 nm. It also implies that the structures of DNA nanotubes are very stable in all three different systems.

To investigate the effect of encapsulated CNTs to structure of DNA nanotubes more deeply, the angle distribution of base in nucleotide to the vertical axial of CNTs (see Supporting Information Section II) were calculated from the last 10 ns simulation in three different systems (see Fig. 3C). The majority of the angle distribution range from 85.8° to 103.4° in three different systems. Meanwhile, in the angle distribution in the system with positive charged CNT, the majority of the angle distribution also ranges from 85.8° to 103.4°. These results show that the angle distributions of nucleotides of DNA nanotubes to the *z* axis are almost the same in three different systems. From the results of Gao's and our papers [50,51], the DNA structure were deformed after the encapsulation or wrapping process of DNA into CNTs. Herein, the majority of angle distribution ranges from 85.8° to 103.4° with the CNT insertion (positive charged CNT) or not (negative charged CNT). It implied the DNA nanotubes structure were very stable even after the encapsulation of CNTs into its hollow. From the data of Fig. 4, one can see the density distribution of Na^+ ion in the *x*-*y* plane are definitely different in different systems, and the abscissa is the distance of Na^+ or other atoms to COM of CNT in *x*-*y* plane. In the negative charged CNT, the distribution of Na^+ has three very sharp peaks. Therein, the first peak value of Na^+ ion is as high as 5.01 in the 0.60 nm region, and the second peak value is as high as 3.82 near 1.40 nm region. The peaks of Na^+ ion are not so sharp and much more flat in the system of positive charged CNTs. The first peak value is less than 2.00 in the region from 2.12 nm to 3.48 nm. It could be understood that the Na^+ ion has been repelled by positive charged CNTs but attracted by the negative charged CNTs. However, the distribution of oxygen atom (O3′ atom) and phosphorus atoms (P atom) of DNA to the axis of CNTs are almost the same in three different systems. It imply that the structure of hexamer DNA nanotubes are very stable in all three different systems even the distribution of ions are different.

CNT (6, 6) has a smaller diameter comparing with CNT (15, 15), and it was also be chosen to investigate the encapsulation process of CNT (with different charge density, namely $\sigma = -0.5\ e/nm^2$, $0\ e/nm^2$ and $+0.5\ e/nm^2$) into DNA nanotubes. Herein, the size of DNA nanotubes is as same as that in the system with CNT (15, 15). The initial structure of the system could be found in Fig. S2 (in the supporting information). To accelerate the encapsulation process, the initial COM distance between CNT (6.6) with different charge density and DNA nanotubes is 3.70 nm, which is smaller than that in system with CNT (15,15). As shown in Fig. 5, the COM distance between CNT with different charge density and DNA nanotubes as a function of simulation time was calculated. The COM distance of

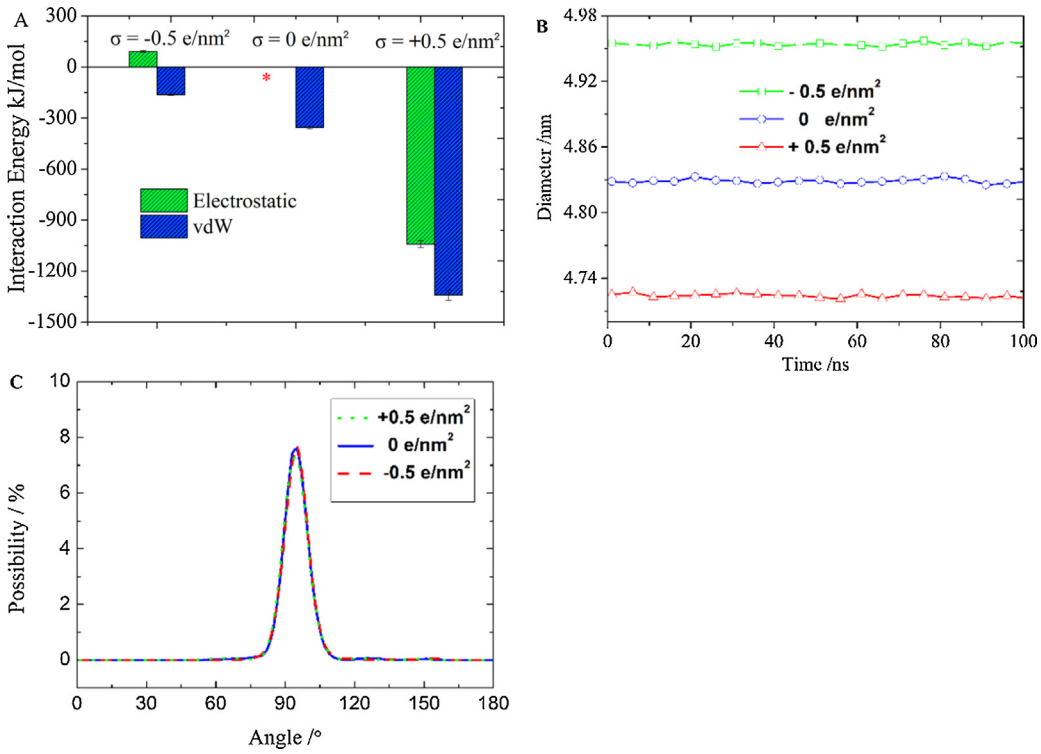

Fig. 3. (A) The average interaction energy between different charged CNT (15,15) and DNA nanotubes in the simulation. The blue one represents the vdW interaction, and green one represents the electrostatic energy, respectively. (B) Evolution of the diameter of hexamer DNA nanotubes during the simulation time in three different systems; (C) The angle distribution of the nucleotide plane of DNA nanotubes and the vertical axis of CNT (*z* axis): positive charged CNT (red line) and neutral CNT (black line). (For interpretation of the references to color in this figure legend, the reader is referred to the web version of this article.)

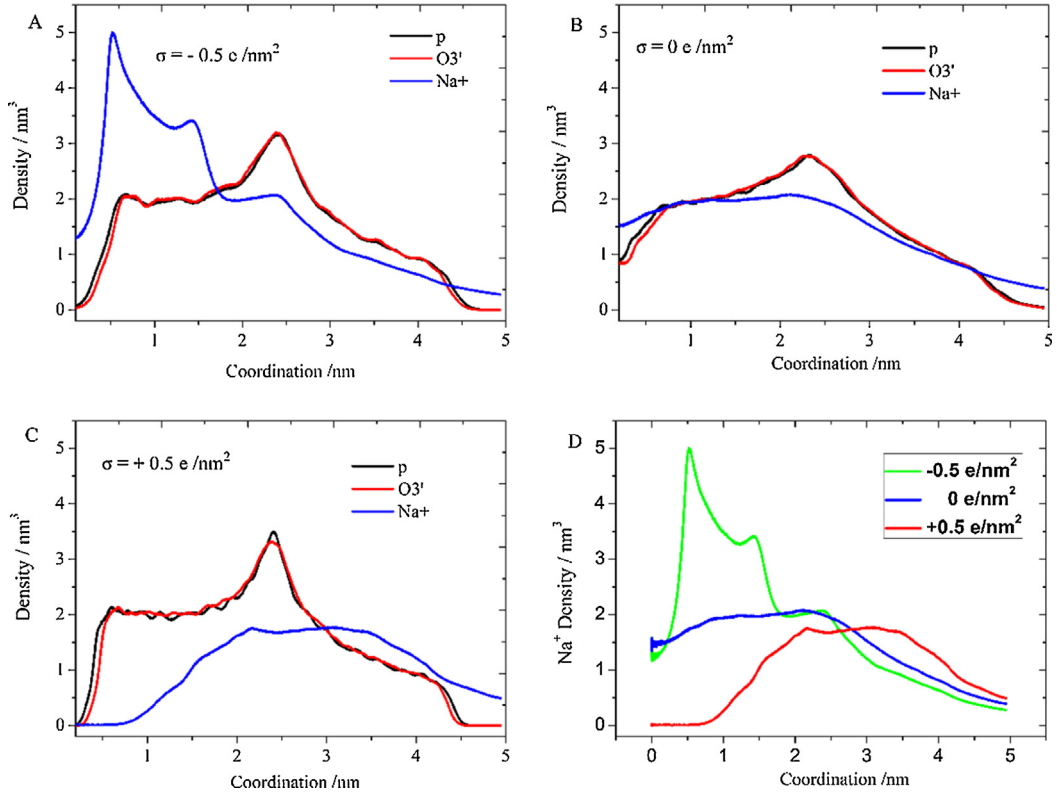

Fig. 4. The density of Na^+ ion, P atom and O3 atom of DNA nanotubes in the *x*-*y* plane with different systems, and the abscissa means the distance of Na^+ to COM of CNT in *x*-*y* plane: (A) $-0.5\,e/nm^2$; (B) $0\,e/nm^2$; (C) $0.5\,e/nm^2$. (D): The Na^+ density in different systems.

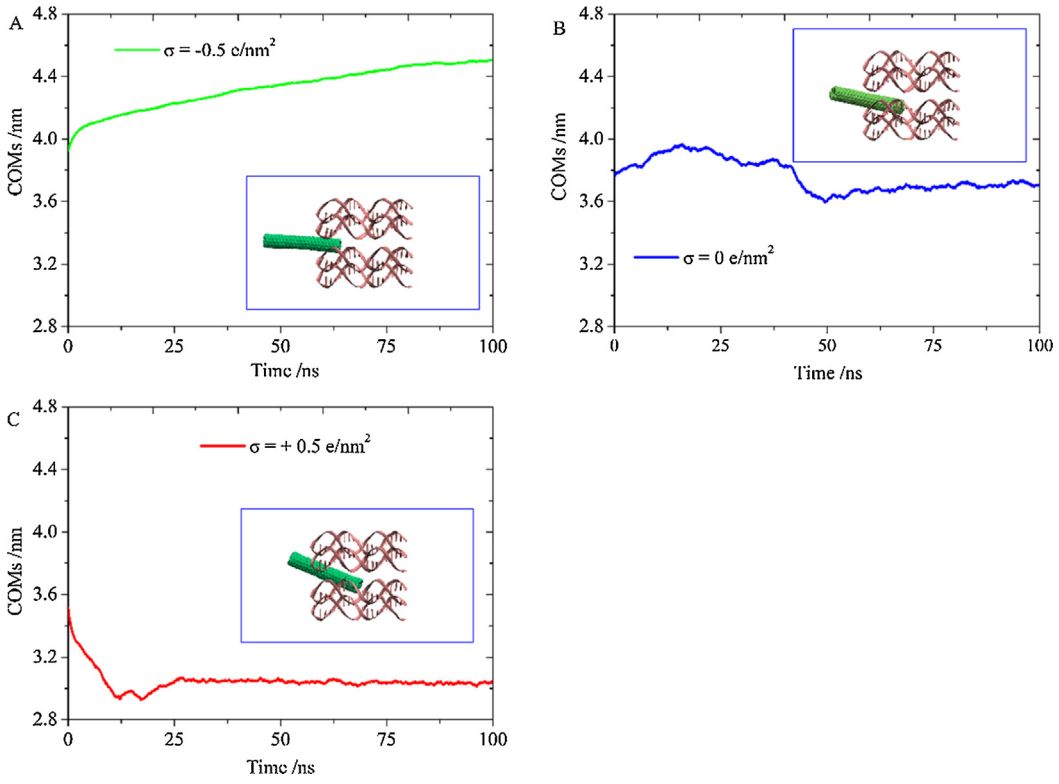

Fig. 5. Evolution of distance between COM of CNT (6, 6) and hexamer DNA nanotubes in the simulation time: (A) $\sigma = -0.5$ e/nm^2; (B) $\sigma = 0$ e/nm^2; (C) $\sigma = 0.5$ e/nm^2.

negative charged CNT and DNA nanotubes increases with the simulation time. The negative charged CNT (6, 6) was repelled by the DNA nanotubes since the DNA nanotubes are naturally negative charged. The encapsulation process of positive charged CNT (6, 6) into DNA nanotubes is not as same as that of positive charged CNT (15, 15). At the beginning of the process, the encapsulation process of positive charged CNT (6, 6) by DNA nanotubes is almost as same as that of positive charged CNT (15, 15). As shown in Fig. 5C, it entered into the hollow of DNA nanotubes rapidly, and the COM distance decrease from 3.52 nm to ca. 2.92 nm.

After that, the insertion process of positive charged CNT (6, 6) to DNA nanotubes is different from that of positive charged CNT (15, 15). The COM distance between positive charged CNT (6, 6) and DNA nanotubes increased from 2.92 nm to 3.05 nm in the simulation from 20.1 ns to 25.8 ns. In this process, the axis of positive charged CNT (6, 6) tends to tile due to the strong interaction between DNA nanotubes and positive charged CNT (6, 6). After that, the system reached a *meta*-stable state, and the positive charge CNT (6, 6) remained in that region in the rest of the simulation time. It demonstrated that a suitable diameter of CNT is significantly important for the successful spontaneous encapsulation process of CNTs into DNA nanotubes.

To obtain a more quantitative picture of the effect of charge on the CNT to the encapsulation process, we performed additional simulations to compute PMF of CNT (15, 15) at different position of DNA nanotubes (see Supporting information Section III). The reaction coordination is the distance between the COM of CNTs and the COM of the DNA nanotubes in z direction. As displayed in Fig. 6, the ΔG decreased from state at $z = 0$ nm (encapsulation state) to the lowest state at $z = 4.60$ nm to 5.40 nm for pristine CNT(15, 15). It implied that pristine CNT (15, 15) favored to escape from encapsulation state by DNA nanotubes. It is easy for CNT (15, 15) to trap at the location at $z = 5.0$ nm since the ΔG is ca. -72.4 ± 7.4 kJ mol^{-1}. In our 100 ns simulation, the pristine CNT (15, 15) was trapped in the DNA nanotubes with the distance $z = 5.23$ nm and it matched the PMF profile very well. On the other hand, for system with positive charged CNT, the ΔG from $z = 0.00$ nm (encapsulation state) to $z = 7.50$ nm (separated state) increased much. It clearly shows that it is very stable for positive CNT (15,15) to be encapsulated by DNA nanotubes. The encapsulation process of pristine CNT (15,15) into DNA nanotubes were not observed in our simulation due to the limitation of simulation time scale. The time of the encapsulation process of pristine CNT (15,15) by DNA nanotubes were estimated based on the references [52,53]. Following Berendsen and Marrink's paper [50], the position-dependent diffusion coefficient D_z in encapsulation process has been calculated. Although the diffusion coefficient of CNT is expected to be position-dependent, this variation is not of primary interest here as that of obtaining an order of magnitude estimate of $<\tau>$. Since the pristine CNT mostly trapped in the region of $z = 4.60$–5.40 nm during the encapsulation process, we computed D_z of CNT at point $z = 5.00$ nm, and it is $(1.5 \pm 0.6) \times 10^{-10}$ m^2/s. Combined with the results of the free energy profile and the diffusion coefficient D_z, the encapsulation time could be estimated as in Eq. (2) [49]:

$$<\tau> = \frac{1}{D_z} \int_{0nm}^{7.5nm} e^{PMF(y)/k_BT} dy \int_{0nm}^{y} e^{-PMF(z)/k_BT} dz \qquad (2)$$

The mean encapsulation time of pristine CNT into DNA nanotubes was estimated to be 21.9. It is 8 orders of magnitude larger compared with our simulation scale. It implies that the encapsulation of pristine CNT by DNA nanotubes is a relatively long process and it decrease by 9 orders of magnitude with the change of pristine CNT to positive charged CNT.

4. Conclusions

In summary, we investigate the charge tunable encapsulation process of CNT into DNA nanotubes. It is very easy for the positive CNT with a suitable diameter to be encapsulated by DNA nanotubes completely. Comparing with the positive CNT, the pristine CNT is

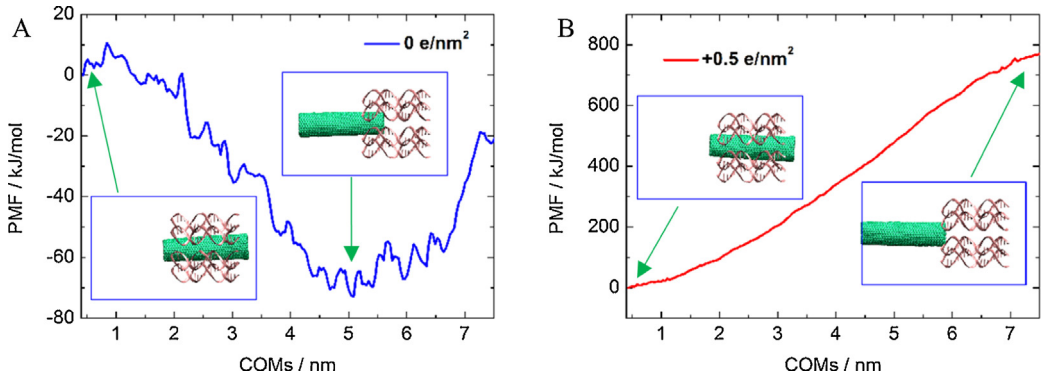

Fig. 6. The potential of mean force (PMF) of encapsulation of CNT (15,15) into DNA nanotubes: (A) pristine CNT; (B) positive charged CNT. The COMs is the distance between the COM of CNT and the COM of the DNA nanotubes in *z* direction.

much more difficult to be encapsulated by DNA nanotubes. The time of the encapsulated process of pristine CNT into DNA nanotubes was estimated on the order of second scale. We also discovered that the structure of DNA nanotubes could still be stable even after the insertion of CNTs into DNA nanotubes. These findings highlight the effect of the charge on the interaction between CNT and DNA nanotubes. It reveals the charge-tunable self-assembly process of nanomaterials and biomolecules. These founding provide the possibility of supplying a building block composited of hybrid CNT-DNA nanotubes for the potential applications in biosensor, drug delivery system and biomaterials.

Conflict of interest

The authors declare no competing financial interest.

Acknowledgements

We acknowledges financial support by the National Natural Science Foundation of China (Grant Nos. 21503186, 21403049, 21273200 and J1210042), Zhejiang Provincial Natural Science Foundation of China (Grant Nos. LY14B030008, LY13F040006, LY15E030009), start funding of Hangzhou Normal University (No. PE13002004041).

Appendix A. Supplementary data

Supplementary data associated with this article can be found, in the online version, at http://dx.doi.org/10.1016/j.jmgm.2016.03.006.

References

[1] N. Enkin, E. Sharon, E. Golub, I. Willner, Nano Lett. 14 (8) (2014) 4918–4922.
[2] J.H. Noh, S.H. Im, J.H. Heo, T.N. Mandal, S.I. Seok, Nano Lett. 13 (4) (2013) 1764–1769.
[3] C. Sanchez, B. Julian, P. Belleville, M. Popall, J. Mater. Chem. 15 (35–36) (2005) 3559–3592.
[4] N.C. Seeman, J. Theor. Biol. 99 (2) (1982) 237–247.
[5] C. Richard, F. Balavoine, P. Schultz, T.W. Ebbesen, C. Mioskowski, Science 300 (5620) (2003) 775–778.
[6] Z. Wei, M. Wan, T. Lin, L. Dai, Adv. Mater. 15 (2) (2003) 136–139.
[7] S.G. Rao, L. Huang, W. Setyawan, S. Hong, Nature 425 (6953) (2003) 36–37.
[8] S. Ahn, A. Choe, J. Park, H. Kim, J.G. Son, S.-S. Lee, M. Park, H. Ko, J. Mater. Chem. C 3 (10) (2015) 2319–2325.
[9] G. Fichman, E. Gazit, Acta Biomater. 10 (4) (2014) 1671–1682.
[10] T. Jiang, C. Xu, X. Zuo, V.P. Conticello, Angew. Chem. Int. Ed. 53 (32) (2014) 8367–8371.
[11] B. Sarkar, L.E.R. O'Leary, J.D. Hartgerink, J. Am. Chem. Soc. 136 (41) (2014) 14417–14424.
[12] H. Yan, S.H. Park, G. Finkelstein, J.H. Reif, T.H. LaBean, Science 301 (5641) (2003) 1882–1884.
[13] E. Winfree, F. Liu, L.A. Wenzler, N.C. Seeman, Nature 394 (6693) (1998) 539–544.
[14] C. Mao, T.H. LaBean, J.H. Reif, N.C. Seeman, Nature 407 (6803) (2000) 493–496.
[15] S. Woo, P.W.K. Rothemund, Nat. Commun. 5 (2014) 4889.
[16] A. Kuzuya, R. Wang, R. Sha, N.C. Seeman, Nano Lett. 7 (6) (2007) 1757–1763.
[17] J.C. Mitchell, J.R. Harris, J. Malo, J. Bath, A.J. Turberfield, J. Am. Chem. Soc. 126 (50) (2004) 16342–16343.
[18] H. Zheng, M. Xiao, Q. Yan, Y. Ma, S.-J. Xiao, J. Am. Chem. Soc. 136 (29) (2014) 10194–10197.
[19] B. Teshome, S. Facsko, A. Keller, Nanoscale 6 (3) (2014) 1790–1796.
[20] C.E. Castro, H.-J. Su, A.E. Marras, L. Zhou, J. Johnson, Nanoscale 7 (14) (2015) 5913–5921.
[21] T.H. LaBean, H. Li, Nano Today 2 (2) (2007) 26–35.
[22] T. Zhang, A. Neumann, J. Lindlau, Y. Wu, G. Pramanik, B. Naydenov, F. Jelezko, F. Schüder, S. Huber, M. Huber, J. Am. Chem. Soc. 137 (31) (2015) 9776–9779.
[23] S.-S. Jester, M. Famulok, Acc. Chem. Res. 47 (6) (2014) 1700–1709.
[24] H. Chen, T.-W. Weng, M.M. Riccitelli, Y. Cui, J. Irudayaraj, J.H. Choi, J. Am. Chem. Soc. 136 (19) (2014) 6995–7005.
[25] S. Hernaíndez-Ainsa, K. Misiunas, V.V. Thacker, E.A. Hemmig, U.F. Keyser, Nano Lett. 14 (3) (2014) 1270–1274.
[26] E. Pfitzner, C. Wachauf, F. Kilchherr, B. Pelz, W.M. Shih, M. Rief, H. Dietz, Angew. Chem. Int. Ed. 125 (30) (2013) 7920–7925.
[27] S. Iijima, Nature 354 (6348) (1991) 56–58.
[28] T. Zhu, B. Xia, L. Zhou, X.W.D. Lou, J. Mater. Chem. 22 (16) (2012) 7851–7855.
[29] D.N. Futaba, K. Hata, T. Yamada, T. Hiraoka, Y. Hayamizu, Y. Kakudate, O. Tanaike, H. Hatori, M. Yumura, S. Iijima, Nat. Mater. 5 (12) (2006) 987–994.
[30] M.F.L. De Volder, S.H. Tawfick, R.H. Baughman, A.J. Hart, Science 339 (6119) (2013) 535–539.
[31] A. Gholizadeh, S. Shahrokhian, A. Iraji zad, S. Mohajerzadeh, M. Vosoughi, S. Darbari, J. Koohsorkhi, M. Mehran, Anal. Chem. 84 (14) (2012) 5932–5938.
[32] M. Steiner, M. Engel, Y.-M. Lin, Y. Wu, K. Jenkins, D.B. Farmer, J.J. Humes, N.L. Yoder, J.-W.T. Seo, A.A. Green, Appl. Phys. Lett. 101 (5) (2012) 053123.
[33] C. Zhou, S. Wang, J. Sun, N. Wei, L. Yang, Z. Zhang, J. Liao, L.-M. Peng, Appl. Phys. Lett. 102 (10) (2013) 103102.
[34] C.-L. Cheng, G.-J. Zhao, Nanoscale 4 (7) (2012) 2301–2305.
[35] H.T. Maune, S.-P. Han, R.D. Barish, M. Bockrath, W.A. Goddard III, P.W.K. Rothemund, E. Winfree, Nat. Nanotech. 5 (1) (2010) 61–66.
[36] D. Roxbury, J. Mittal, A. Jagota, Nano Lett. 12 (3) (2012) 1464–1469.
[37] X.J. Zhao, Phys. Chem. C 115 (14) (2011) 6181–6189.
[38] Q. Hang, Q. Jiang, N. Li, et al., ACS Nano 8 (7) (2014) 6633–6643.
[39] L. Meng, X. Zhang, Q. Lu, et al., Biomaterials 33 (6) (2012) 1689–1698.
[40] W. Humphrey, A. Dalke, K.J. Schulten, Mol. Graph. Model. 14 (1) (1996) 33–38.
[41] L.T. Zhuravlev, Colloids Surf. A: Physicochem. Eng. Aspects 173 (1) (2000) 1–38.
[42] M. Shankla, A. Aksimentiev, Nat. Commun. 5 (2014) 5171.
[43] Z. Kong, W. Zheng, Q. Wang, H. Wang, F. Xi, L. Liang, J.-W. Shen, J. Mater. Chem. B 3 (2015) 4814–4820.
[44] J. Yoo, A. Aksimentiev, Proc. Natl. Acad. Sci. U. S. A. 110 (50) (2013) 20099–20104.
[45] J.-W. Shen, T. Wu, Q. Wang, Y. Kang, Biomaterials 29 (28) (2008) 3847–3855.
[46] Z. Zhang, J. Shen, H. Wang, Q. Wang, J. Zhang, L. Liang, H. Ågren, Y.J. Tu, Phys. Chem. Lett. 5 (9) (2014) 1602–1607.
[47] Y. Kang, Z. Zhang, H. Shi, J. Zhang, L. Liang, Q. Wang, H. Ågren, Y. Tu, Nanoscale 6 (18) (2014) 10666–10672.
[48] Z.-S. Zhang, Y. Kang, L.-J. Liang, Y.-C. Liu, T. Wu, Q. Wang, Biomaterials 35 (5) (2014) 1771–1778.
[49] T. Darden, D. York, L. Pedersen, J. Phys. Chem. 98 (12) (1993) 10089–10092.
[50] H. Gao, Y. Kong, D. Cui, C.S. Ozkan, Nano Lett. 3 (4) (2003) 471–473.
[51] J.-W. Shen, T. Tang, X.-H. Wei, W. Zheng, T.-Y. Sun, Z. Zhang, L. Liang, Q. Wang, RSC Adv. 5 (70) (2015) 56896–56903.
[52] S.J. Marrink, H.J.C. Berendsen, J. Phys. Chem. 100 (41) (1996) 16729–16738.
[53] R. Qiao, A.P. Roberts, A.S. Mount, S.J. Klaine, P.C. Ke, Nano Lett. 7 (3) (2007) 614–619.